



Contents lists available at ScienceDirect

Biochemical Pharmacology

journal homepage: www.elsevier.com/locate/biochempharm



Novel third-generation water-soluble noscapine analogs as superior microtubule-interfering agents with enhanced antiproliferative activity

Maged Henary^{a,*}, Lakshminarayana Narayana^{a,b}, Shazia Ahad^c, Sushma R. Gundala^b, Rao Mukkavilli^d, Vibhuti Sharma^b, Eric A. Owens^a, Yogesh Yadav^{a,b}, Mulpuri Nagaraju^a, Donald Hamelberg^a, Vibha Tandon^{e,f}, Dulal Panda^c, Ritu Aneja^{b,**}

^a Department of Chemistry and Biochemistry, Georgia State University, Petit Science Center, 100 Piedmont Ave., Atlanta, GA 30303, USA

^b Department of Biology, Georgia State University, Petit Science Center, 100 Piedmont Ave., Atlanta, GA 30303, USA

^c Department of Biosciences and Bioengineering, Indian Institute of Technology Bombay, Mumbai 400076, India

^d Advinus Therapeutics Limited, Bangalore, Karnataka, India

^e Department of Chemistry, University of Delhi, India

^f Special Centre of Molecular Medicine, Jawaharlal Nehru University, Delhi, India

ARTICLE INFO

Article history:

Received 18 June 2014

Accepted 21 July 2014

Available online xxx

Keywords:

Noscapine

Water solubility

Tubulin binding

Antiproliferative

Pharmacokinetics

ABSTRACT

Noscapine, an opium-derived 'kinder-gentler' microtubule-modulating drug is in Phase I/II clinical trials for cancer chemotherapy. However, its limited water solubility encumbers its development into an oral anticancer drug with clinical promise. Here we report the synthesis of 9 third-generation, water-soluble noscapine analogs with negatively charged sulfonate and positively charged quaternary ammonium groups using noscapine, 9-bromonoscapine and 9-aminonoscapine as scaffolds. The predictive free energy of solvation was found to be lower for sulfonates (**6a–c**; **8a–c**) compared to the quaternary ammonium-substituted counterparts, explaining their higher water solubility. In addition, sulfonates showed higher charge dispersability, which may effectively shield the hydrophobicity of isoquinoline nucleus as indicated by hydrophobicity mapping methods. These *in silico* data underscore efficient net charge balancing, which may explain higher water solubility and thus enhanced antiproliferative efficacy and improved bioavailability. We observed that **6b**, **8b** and **8c** strongly inhibited tubulin polymerization and demonstrated significant antiproliferative activity against four cancer cell lines compared to noscapine. Molecular simulation and docking studies of tubulin-drug complexes revealed that the brominated compound with a four-carbon chain (**4b**, **6b**, and **8b**) showed optimal binding with tubulin heterodimers. Interestingly, **6b**, **8b** and **8c** treated PC-3 cells resulted in preponderance of mitotic cells with multipolar spindle morphology, suggesting that they stall the cell cycle. Furthermore, *in vivo* pharmacokinetic evaluation of **6b**, **8b** and **8c** revealed at least 1–2-fold improvement in their bioavailability compared to noscapine. To our knowledge, this is the first report to demonstrate novel water-soluble noscapine analogs that may pave the way for future pre-clinical drug development.

© 2014 Elsevier Inc. All rights reserved.

1. Introduction

Over the past few decades, microtubule-active drugs have met with abundant success in the oncology clinic for a wide-spectrum of malignancies [1,2]. Beyond the two major classes of tubulin-binding drugs, namely, vincas (that depolymerize microtubules)

and taxanes (that overpolymerize microtubules), the "middle-path" drugs such as noscapine, 2-ME, griseofulvin, are currently a topic of intense investigation both for their clinical utility as well as from a mechanistic standpoint [2–4]. Essentially, these "middle-path" drugs do not overpolymerize or depolymerize microtubules over a broad concentration range, rather subtly attenuate microtubule dynamics. Unlike microtubule polymerizing (taxanes) or microtubule depolymerizing (vincas) drugs, these middle-path agents are also referred to as microtubule modulating drugs (noscapines). They withstand the harsh effects on the microtubules over a wide span of concentration by increasing the pause phase of

* Corresponding author.

** Corresponding author. Tel. +1 404 413 5417.

E-mail address: raneja@gsu.edu (R. Aneja).

microtubules, which in turn, helps them offer a wider therapeutic window with lower toxicity than classical tubulin binding drugs. No wonder microtubule-drugs currently occupy a major segment of the ever-expanding armamentarium of clinical chemotherapeutic regimens. Nonetheless, several impediments associated with their clinical use, such as non-specific toxicity, drug resistance, and water insolubility, have resulted in a sub-optimal realization of their clinical potential [5,6]. Thus, in the wake of these pharmacological challenges, new anticancer drug discovery, synthesis and development constitute an active area of intense research.

Noscapine, an innocuous cough-suppressant, was identified for its previously unrecognized tubulin-binding activity and chemotherapeutic benefits in the late 1990s [7,8]. The promising anticancer activity of noscapine coupled with its non-toxic attributes facilitated its quick inclusion into Phase 1/2 clinical trials [9]. Ever since, several groups including ours, have been actively engaged in the synthesis of *in silico* guided, more potent noscapine analogs with potentially better pharmacological profiles [10,11]. Recently, we reported the synthesis of second-generation 7-position benzofuranone noscapine analogs that offered better antiproliferative activity than the founding molecule [12–14]. Although first-pass *in vitro* experiments remain feasible with several more potent synthetic noscapine analogs, water insolubility has emerged to be a major issue for *in vivo* experimentation. Essentially, diminution of aqueous solubility can be ascribed to the presence of substituted isoquinoline and isobenzofuranone ring systems, which confer highly hydrophobic structural characteristics. This lack of adequate solubility thus poses a challenge for further drug development as low water solubility directly impacts absorption and distribution profiles of the test agents, thus compromising bioavailability. Thus the solubility characteristics of a drug are profoundly crucial at early drug development stage, in particular for animal studies. Given that the partition coefficient and TPSA (Topological Polar Surface Area) are the main descriptors of aqueous solubility of a drug, integrating knowledge of these parameters is often sought for fine-tuning the physicochemical profiles of drugs.

Here we describe rational design, and chemical modification of noscapine and its known congeners to successfully yield novel water-soluble analogs by incorporation of certain charged functional groups namely alkyl quaternary ammonium salt and alkyl sulfonates. Our data demonstrate that introduction of a charged species on the noscapine core greatly improved aqueous solubility, which reflected as enhanced bioavailability compared to noscapine and *in vitro* efficacy in reducing the proliferation of cancer cells. These data offer compelling grounds to further investigate the preclinical activity and pharmacokinetics of these novel water-soluble noscapine analogs.

2. Materials and methods

2.1. General

NMR spectroscopy was performed on a Bruker Avance (400 MHz) spectrometer located in the Department of Chemistry NMR facility and the solvents for the NMR experiments (99.8% CD₃OD-*d*₄, DMSO-*d*₆ and CDCl₃) were obtained from Cambridge Isotope Laboratories (Andover, MA) including TMS as the internal calibration standard. The reactions were followed using silica gel 60 F₂₅₄ thin layer chromatography plates (Merck EMD Millipore, Darmstadt, Germany). Open column chromatography was utilized for the purification of all final compounds using 60–200 μ m, 60A classic column silica gel (Dynamic Adsorbents, Norcross, GA). The melting points were determined with a Mel-temp melting point apparatus and are given as uncorrected values. High-resolution

accurate mass spectra (HRMS) were obtained either at the Georgia State University Mass Spectrometry Facility using a Waters Q-TOF micro (ESI-Q-TOF) mass spectrometer or utilizing a Waters Micromass LCT TOF ES + Premier Mass Spectrometer. HPLC analyses were carried out on a Waters 1525 Binary HPLC pump/waters 2487 dual absorbance detector system using a Waters Delta-Pak 5 μ m 100A 3.9 \times 150 mm reversed phase C₁₈ column. All reported yields refer to pure isolated compounds. Chemical and solvents were of reagent grade and used as obtained from Alfa Aesar (Ward Hill, MS) and Sigma Aldrich (St. Louis, MO) without further purification. The determined purity of all the final synthesized compounds were >95% as estimated by HPLC or determined by elemental analysis.

2.2. Chemical synthesis

2.2.1. (S)-3-((R)-9-bromo-4-methoxy-6-methyl-5,6,7,8-tetrahydro-[1,3]dioxolo[4,5-g]isoquinolin-5-yl)-6,7-dimethoxyisobenzofuran-1(3H)-one (2)

(S)-3-((R)-9-bromo-4-methoxy-6-methyl-5,6,7,8-tetrahydro-[1,3]dioxolo[4,5-g]isoquinolin-5-yl)-6,7-dimethoxyisobenzofuran-1(3H)-one (2) was synthesized from 1 and 1.4 g was obtained in 82% yield following the reported procedure [12].

2.2.2. (S)-3-((R)-9-amino-4-methoxy-6-methyl-5,6,7,8-tetrahydro-[1,3]dioxolo[4,5-g]isoquinolin-5-yl)-6,7-dimethoxyisobenzofuran-1(3H)-one (3)

Sodium azide (0.99 g, 15.231 mmoles, 2 equiv) was added to a solution of 9-bromo noscapine (3.0 g, 6.092 mmoles) in anhydrous DMSO (20 mL) followed by the addition of Cu₂O (872 mg, 6.092 mmoles, 1.0 equiv) and L-proline (912 mg, 7.917 mmoles, 1.3 equiv). The reaction mixture was stirred at 100 °C for 24 h while monitoring by TLC. The mixture was then quenched by the addition of aq. NH₄Cl solution and was extracted with DCM (2 \times 60 mL). The organic layer was then washed with water (2 \times 30 mL), dried over anhydrous Na₂SO₄, concentrated and purified by flash chromatography to obtain 2.1 g of the desired product. Yield: 81%; mp: 124 °C; ¹H NMR (400 MHz, CD₃OD) δ : 7.21 (d, *J* = 8.0 Hz, 1H), 6.24 (d, *J* = 8.4 Hz, 1H), 5.95 (s, 2H), 5.67 (s, 1H), 4.41 (s, 1H), 3.98 (s, 3H), 3.88 (s, 3H), 3.86 (s, 3H), 2.62 (t, *J* = 4.0 Hz, 1H), 2.48 (s, 3H), 2.45 (m, 2H), 1.83 (m, 1H); ¹H NMR (400 MHz, CDCl₃) δ : 6.96 (d, *J* = 8.0 Hz, 1H), 6.16 (d, *J* = 8.4 Hz, 1H), 5.93 (d, *J* = 2.0 Hz, 2H), 5.61 (d, *J* = 3.6 Hz, 1H), 4.37 (d, *J* = 4.0 Hz, 1H), 4.07 (s, 3H), 3.87 (s, 3H), 3.86 (s, 3H), 3.79 (br s, 2H), 2.60 (m, 1H), 2.51 (s, 3H), 2.45 (m, 1H), 2.35 (m, 1H), 1.70 (m, 1H); ¹³C NMR (100 MHz, CDCl₃) δ : 168.7, 152.4, 147.1, 141.0, 134.5, 133.1, 132.2, 121.2, 119.8, 118.1, 117.3, 116.2, 101.8, 82.3, 63.6, 61.1, 60.0, 57.4, 49.2, 46.3, 20.0; HRMS (M + H)⁺: *m/z* Calcd. for C₂₂H₂₅N₂O₇, 429.1662; found 429.1646.

2.2.3. 3-(((R)-5-((S)-4,5-dimethoxy-3-oxo-1,3-dihydroisobenzofuran-1-yl)-4-methoxy-6-methyl-5,6,7,8-tetrahydro-[1,3]dioxolo[4,5-g]isoquinolin-9-yl)amino)-N,N,N-trimethylpropan-1-aminium bromide (4a)

Triethyl amine (0.7 mL, 4.67 mmoles) was added to a solution of 9-amino noscapine (1.0 g, 2.335 mmoles) in anhydrous DMF (10 mL) followed by the addition of 3-bromopropyltrimethylammoniumbromide (609.2 mg, 2.335 mmoles) and the reaction mixture was stirred at 90 °C for 17 h while monitoring by TLC. The reaction mixture was then concentrated at 60 °C under reduced pressure and the crude product was purified by flash chromatography to obtain 820 mg of the desired product. Yield: 67%; mp: 48 °C; ¹H NMR (400 MHz, CD₃OD) δ : 7.29 (d, *J* = 8.4 Hz, 1H), 6.58 (d, *J* = 8.0 Hz, 1H), 5.89 (d, *J* = 2.8 Hz, 2H), 5.69 (d, *J* = 2.8 Hz, 1H), 4.44 (d, *J* = 3.2 Hz, 1H), 3.95 (s, 3H), 3.90 (s, 3H), 3.70 (s, 3H), 3.48 (dt, *J* = 2.0 Hz and 8.0 Hz, 2H), 3.35 (t, *J* = 8.0 Hz, 2H), 3.15 (s, 9H), 2.91

(m, 1H), 2.59 – 2.52 (m, 2H), 2.53 (s, 3H), 2.05 – 2.00 (m, 3H); ¹³C NMR (100 MHz, CD₃OD): 168.6, 152.6, 147.2, 140.7, 136.7, 135.4, 133.9, 124.4, 119.5, 119.4, 118.8, 115.3, 100.6, 81.1, 64.7, 61.11, 61.00, 58.7, 56.1, 55.7, 55.7, 52.5, 52.4, 46.0, 43.6, 42.6, 24.0, 21.4, 6.7; HRMS (M)⁺: *m/z* Calcd. for C₂₈H₃₈N₃O₇, 528.2710; found 528.2726.

2.2.4. 4-(((R)-5-((S)-4,5-dimethoxy-3-oxo-1,3-dihydroisobenzofuran-1-yl)-4-methoxy-6-methyl-5,6,7,8-tetrahydro-[1,3]dioxolo[4,5-g]isoquinolin-9-yl)amino)butane-1-sulfonic acid (4b)

1,4-Butanesultone (318 mg, 2.335 mmoles) was added to a solution of 9-amino noscapine (1.0 g, 2.335 mmoles) in anhydrous *i*-propanol (10 mL) and the reaction mixture was refluxed for 17 h while monitoring by TLC. The reaction mixture was concentrated under reduced pressure and the crude product was purified by flash chromatography to obtain 780 mg of the desired product. Yield: 59%; mp: 52 °C; ¹H NMR (400 MHz, CDCl₃) δ: 7.04 (d, *J* = 8.4 Hz, 1H), 6.35 (d, *J* = 7.6 Hz, 1H), 5.84 (d, *J* = 7.6 Hz, 2H), 5.57 (d, *J* = 3.2 Hz, 1H), 4.40 (d, *J* = 2.8 Hz, 1H), 4.05 (s, 3H), 3.78 (s, 3H), 3.70 (s, 3H), 3.50 (m, 2H), 3.36 (m, 2H), 3.15 (m, 1H), 2.95 (m, 3H), 2.50 (s, 3H), 1.85 (m, 2H), 1.60 (m, 2H); ¹³C NMR (100 MHz, CDCl₃) δ: 168.0, 152.3, 147.5, 140.9, 137.1, 135.3, 134.2, 124.8, 119.8, 119.3, 118.7, 118.1, 100.6, 81.3, 71.5, 67.5, 62.2, 61.2, 59.4, 56.9, 51.0, 48.5, 46.2, 44.8, 29.7, 29.5, 29.0, 22.1, 21.9, 21.4; HRMS (M + H)⁺: *m/z* Calcd. for C₂₆H₃₃N₂O₁₀S, 565.1856; found 565.1831.

2.2.5. 3-(((R)-5-((S)-4,5-dimethoxy-3-oxo-1,3-dihydroisobenzofuran-1-yl)-4-methoxy-6-methyl-5,6,7,8-tetrahydro-[1,3]dioxolo[4,5-g]isoquinolin-9-yl)amino)propane-1-sulfonic acid (4c)

1,3-Propanesultone (285 mg, 2.335 mmoles) was added to a solution of 9-amino noscapine (1.0 g, 2.335 mmoles) in anhydrous *i*-propanol (10 mL) and the reaction mixture was refluxed for 17 h while monitoring by TLC. The solvent was then evaporated from the reaction mixture under reduced pressure and the crude product was purified by flash chromatography to obtain 750 mg of the desired product. Yield: 58%; mp: 55 °C; ¹H NMR (400 MHz, CD₃OD) δ: 7.34 (d, *J* = 8.0 Hz, 1H), 6.13 (d, *J* = 8.0 Hz, 1H), 5.93 (d, *J* = 7.4 Hz, 2H), 5.64 (s, 1H), 4.49 (s, 1H), 3.97 (s, 3H), 3.90 (s, 3H), 3.88 (s, 3H), 3.57 (m, 1H), 3.40 (m, 1H), 3.30 (m, 1H), 2.80 (m, 2H), 2.60 (m, 1H), 2.55 (s, 3H), 2.45 (m, 1H), 2.00 (m, 2H), 1.75 (m, 1H); ¹³C NMR (100 MHz, CDCl₃) δ: 168.9, 152.6, 147.2, 140.2, 137.1, 135.6, 134.0, 124.3, 120.1, 119.3, 119.2, 118.2, 116.1, 100.6, 81.6, 71.5, 66.3, 61.0, 60.9, 58.9, 56.1, 48.9, 44.7, 44.6, 25.6, 25.4, 21.8, 21.1; HRMS (M + H)⁺: *m/z* Calcd. for C₂₅H₃₁N₂O₁₀S, 551.1699; found 551.1686.

2.2.6. (S)-7-hydroxy-6-methoxy-3-((R)-4-methoxy-6-methyl-5,6,7,8-tetrahydro-[1,3]dioxolo[4,5-g]isoquinolin-5-yl)isobenzofuran-1(3H)-one (5)

(S)-7-hydroxy-6-methoxy-3-((R)-4-methoxy-6-methyl-5,6,7,8-tetrahydro-[1,3]dioxolo[4,5-g]isoquinolin-5-yl)isobenzofuran-1(3H)-one (5) was prepared by reported procedure in comparable yield [14].

2.2.7. 3-(((S)-5-methoxy-1-((R)-4-methoxy-6-methyl-5,6,7,8-tetrahydro-[1,3]dioxolo[4,5-g]isoquinolin-5-yl)-3-oxo-1,3-dihydroisobenzofuran-4-yl)oxy)-N,N,N-trimethylpropan-1-aminium bromide (6a)

Potassium carbonate (464 mg, 6.70 mmoles) was added to a solution of 7-hydroxy noscapine (1.34 g, 3.35 mmoles) in anhydrous DMF (10 mL) followed by the addition of 3-bromopropyl-trimethyl-ammoniumbromide (876 mg, 3.35 mmoles) and the reaction mixture was stirred at 90 °C for 6 h while monitoring by TLC. The reaction mixture was then filtered, washed the filter

with DCM, combined the filtrate and washings and evaporated under reduced pressure at 60 °C. The crude product was then purified by flash chromatography to obtain 1.12 g of the desired product. Yield: 67%; mp: 73 °C; ¹H NMR (400 MHz, CD₃OD): δ 7.22 (d, *J* = 8.4 Hz, 1H), 6.36 (s, 1H), 6.22 (d, *J* = 8.0 Hz, 1H), 5.95 (s, 2H), 5.63 (d, *J* = 3.6 Hz, 1H), 4.40 (d, *J* = 3.6 Hz, 1H), 4.35 (m, 1H), 4.26 – 4.24 (m, 1H), 3.99 (s, 3H), 3.90 (s, 3H), 3.86 – 3.84 (m, 2H), 3.25 (s, 9H), 2.65 – 2.61 (m, 1H), 2.53 (s, 3H), 2.50 – 2.46 (m, 1H), 2.42 – 2.40 (m, 1H), 2.28 – 2.23 (m, 2H), 2.02 – 1.97 (m, 1H); ¹³C NMR (100 MHz, CD₃OD) δ: 169.1, 152.6, 148.9, 145.4, 140.7, 140.3, 134.1, 131.8, 119.7, 118.7, 118.5, 115.9, 102.1, 100.9, 81.8, 70.4, 64.3, 64.3, 60.9, 58.6, 55.8, 52.4, 52.4, 52.3, 49.4, 44.9, 27.1, 23.7; HRMS (M)⁺: *m/z* Calcd. for C₂₇H₃₅N₂O₇, 499.2444; found 499.2456.

2.2.8. 4-(((S)-5-methoxy-1-((R)-4-methoxy-6-methyl-5,6,7,8-tetrahydro-[1,3]dioxolo[4,5-g]isoquinolin-5-yl)-3-oxo-1,3-dihydroisobenzofuran-4-yl)oxy)butane-1-sulfonic acid (6b)

Sodium hydride (60 mg, 2.50 mmoles) was added to a solution of 7-hydroxy noscapine (1.0 g, 2.50 mmoles) in anhydrous DMF (10 mL) and the reaction mixture was stirred at room temperature for 30 min. 1,4-Butanesultone (511.7 mg, 3.75 mmoles) was added and the reaction mixture was stirred at 90 °C for 5 h while monitoring by TLC. The mixture was then concentrated under reduced pressure at 60 °C and the crude product was purified by flash chromatography to obtain 940 mg of the desired product. Yield: 70%; mp: 98 °C; ¹H NMR (400 MHz, CD₃OD) δ: 7.21 (d, *J* = 8.4 Hz, 1H), 6.36 (s, 1H), 6.31 (d, *J* = 8.4 Hz, 1H), 5.93 (s, 2H), 5.68 (d, *J* = 3.2 Hz, 1H), 4.51 (d, *J* = 3.2 Hz, 1H), 4.20 – 4.14 (m, 2H), 3.93 (s, 3H), 3.87 (s, 3H), 2.95 (t, *J* = 8.0 Hz, 2H), 2.75 (m, 1H), 2.60 (s, 3H), 2.50 – 2.48 (m, 2H), 2.15 – 2.09 (m, 1H), 2.07 – 2.00 (m, 2H), 1.92 – 1.85 (m, 2H); ¹³C NMR (100 MHz, CDCl₃) δ: 168.4, 152.7, 148.7, 146.7, 140.4, 140.2, 134.0, 131.3, 119.9, 118.6, 117.8, 102.5, 100.9, 81.2, 77.4, 77.3, 77.0, 76.7, 74.2, 60.8, 59.4, 56.8, 50.9, 49.1, 45.4, 28.8, 26.7, 21.0; HRMS (M + H)⁺: *m/z* Calcd. for C₂₅H₃₀NO₁₀S, 536.1590; found 536.1570.

2.2.9. 3-(((S)-5-methoxy-1-((R)-4-methoxy-6-methyl-5,6,7,8-tetrahydro-[1,3]dioxolo[4,5-g]isoquinolin-5-yl)-3-oxo-1,3-dihydroisobenzofuran-4-yl)oxy)propane-1-sulfonic acid (6c)

Sodium hydride (60 mg, 2.50 mmoles) was added to a solution of 7-hydroxy noscapine (1.0 g, 2.50 mmoles) in anhydrous DMF (10 mL) and the reaction mixture was stirred at room temperature for 30 min. 1,3-Propanesultone (511.7 mg, 3.75 mmoles) was then added and the reaction mixture was stirred at 90 °C for 5 h while monitoring by TLC. The mixture was then concentrated under reduced pressure at 60 °C and the crude product was purified by flash chromatography to obtain 876 mg of the desired product. Yield: 67%; mp: 80 °C; ¹H NMR (400 MHz, CD₃OD) δ: 7.22 (d, *J* = 8.4 Hz, 1H), 6.39 – 6.37 (m, 2H), 5.92 (s, 2H), 5.71 (d, *J* = 3.2 Hz, 1H), 4.58 (d, *J* = 2.4 Hz, 1H), 4.24 – 4.20 (m, 2H), 3.90 (s, 3H), 3.87 (s, 3H), 3.11 (t, *J* = 7.6 Hz, 2H), 2.85 – 2.82 (m, 1H), 2.65 (s, 3H), 2.60 – 2.57 (m, 2H), 2.23 – 2.16 (m, 3H); ¹³C NMR (100 MHz, CD₃OD) δ: 168.4, 152.9, 149.2, 146.2, 140.2, 140.0, 134.0, 130.9, 119.4, 118.8, 118.2, 114.3, 102.1, 101.0, 80.8, 73.1, 61.0, 58.6, 55.9, 53.5, 48.8, 44.1, 26.0, 25.6; HRMS (M + H)⁺: *m/z* Calcd. for C₂₄H₂₈NO₁₀S, 522.1434; found 522.1443.

2.2.10. (S)-3-((R)-9-bromo-4-methoxy-6-methyl-5,6,7,8-tetrahydro-[1,3]dioxolo[4,5-g]isoquinolin-5-yl)-7-hydroxy-6-methoxyisobenzofuran-1(3H)-one (7)

(S)-3-((R)-9-bromo-4-methoxy-6-methyl-5,6,7,8-tetrahydro-[1,3]dioxolo[4,5-g]isoquinolin-5-yl)-7-hydroxy-6-methoxyisobenzofuran-1(3H)-one (7) was synthesized in 64% yield starting from compound 2, by adopting the procedure reported for the synthesis of compound 5.

2.2.11. 3-(((S)-1-((R)-9-bromo-4-methoxy-6-methyl-5,6,7,8-tetrahydro-[1,3]dioxolo[4,5-g]isoquinolin-5-yl)-5-methoxy-3-oxo-1,3-dihydroisobenzofuran-4-yl)oxy)-N,N,N-trimethylpropan-1-aminium bromide (**8a**)

Potassium carbonate (578 mg, 4.18 mmoles) was added to a solution of 9-bromo-7-hydroxy noscapine (1.0 g, 2.09 mmoles) in anhydrous DMF (10 mL) followed by the addition of 3-bromopropyl trimethylammoniumbromide (547 mg, 2.09 mmoles) and the reaction mixture was stirred at 90 °C for 6 h while monitoring by TLC. The mixture was then filtered, washed the filter with DCM, combined the filtrate and concentrated under reduced pressure at 60 °C. The crude product was then purified by flash chromatography to afford 847 mg of the desired product. Yield: 70%; mp: 75 °C; ¹H NMR (400 MHz, CD₃OD) δ: 7.31 (d, *J* = 8.4 Hz, 1H), 6.53 (d, *J* = 8.4 Hz, 1H), 6.04 (d, *J* = 7.2 Hz, 2H), 5.65 (d, *J* = 3.2 Hz, 1H), 4.44 (d, *J* = 3.6 Hz, 1H), 4.35 – 4.31 (m, 1H), 4.27 – 4.24 (m, 1H), 3.91 (s, 3H), 3.88 (s, 3H), 3.85 – 3.81 (m, 2H), 3.25 (s, 9H), 2.80 (m, 1H), 2.66 – 2.65 (m, 1H), 2.60 (m, 1H), 2.54 (s, 3H), 2.26 – 2.24 (m, 2H), 2.10 – 2.06 (m, 1H); ¹³C NMR (100 MHz, CD₃OD) δ: 168.7, 152.7, 147.0, 145.6, 140.8, 139.8, 134.3, 129.7, 119.2, 119.0, 118.4, 117.6, 101.5, 95.2, 81.0, 70.6, 64.3, 61.0, 58.77, 56.1, 52.6, 52.6, 52.5, 43.6, 25.4, 23.9; HRMS (M)⁺: *m/z* Calcd. for C₂₇H₃₄BrN₂O₇, 577.1549; found 577.1545.

2.2.12. 4-(((S)-1-((R)-9-bromo-4-methoxy-6-methyl-5,6,7,8-tetrahydro-[1,3]dioxolo[4,5-g]isoquinolin-5-yl)-5-methoxy-3-oxo-1,3-dihydroisobenzofuran-4-yl)oxy)butane-1-sulfonic acid (**8b**)

Sodium hydride (40.2 mg, 1.672 mmoles) was added to a solution of 9-bromo-7-hydroxy noscapine (0.8 g, 1.672 mmoles) in anhydrous DMF (10 mL) and the reaction mixture was stirred at room temperature for 30 min. 1,4-Butanesultone (228 mg, 1.672 mmoles) was added and the reaction mixture was stirred at 90 °C for 5 h while monitoring by TLC. The mixture was then concentrated under reduced pressure at 60 °C and the crude product was purified by flash chromatography to afford 650 mg of the desired product. Yield: 63%; mp: 172 °C; ¹H NMR (400 MHz, CD₃OD, δ): 7.31 (d, *J* = 8.4 Hz, 1H), 6.59 (d, *J* = 8.4 Hz, 1H), 6.04 (s, 2H), 5.72 (d, *J* = 3.2 Hz, 1H), 4.61 (s, 1H), 4.22 – 4.19 (m, 2H), 3.89 (s, 3H), 3.84 (s, 3H), 2.93 (t, *J* = 7.6 Hz, 2H), 2.78 – 2.74 (m, 1H), 2.65 (s, 3H), 2.25 (m, 1H), 2.05 – 2.01 (m, 3H), 1.95 – 1.89 (m, 3H); ¹³C NMR (100 MHz, CD₃OD) δ: 168.2, 153.0, 147.4, 146.5, 140.3, 139.7, 134.2, 129.0, 119.2, 118.9, 118.0, 115.9, 101.5, 95.1, 80.3, 73.8, 61.1, 58.6, 56.0, 53.4, 50.9, 42.8, 28.7, 24.9, 21.2; HRMS (M + H)⁺: *m/z* Calcd. for C₂₅H₂₉BrNO₁₀S, 614.0696; found 614.0700.

2.2.13. 3-(((S)-1-((R)-9-bromo-4-methoxy-6-methyl-5,6,7,8-tetrahydro-[1,3]dioxolo[4,5-g]isoquinolin-5-yl)-5-methoxy-3-oxo-1,3-dihydroisobenzofuran-4-yl)oxy)propane-1-sulfonic acid (**8c**)

Sodium hydride (36 mg, 1.46 mmoles) was added to a solution of 9-bromo-7-hydroxy noscapine (0.7 g, 1.46 mmoles) in anhydrous DMF (10 mL) and the reaction mixture was stirred at room temperature for 30 min. 1,3-Propanesultone (180 mg, 1.46 mmoles) was added and the reaction mixture was stirred at 90 °C for 5 h while monitoring by TLC. The mixture was then concentrated under reduced pressure at 60 °C and the crude product was purified by flash chromatography to afford 620 mg of the desired product. Yield: 71%; mp: 176 °C; ¹H NMR (400 MHz, CD₃OD) δ: 7.28 (d, *J* = 8.0 Hz, 1H), 6.52 (d, *J* = 8.0 Hz, 1H), 6.03 (d, *J* = 4.4 Hz, 1H), 5.68 (s, 1H), 4.54 (s, 1H), 4.30 – 4.25 (m, 2H), 3.88 (s, 3H), 3.87 (s, 3H), 3.13 (t, *J* = 4.8 Hz, 2H), 2.85 – 2.73 (m, 1H), 2.70 – 2.66 (m, 2H), 2.60 (s, 3H), 2.20 – 2.16 (m, 3H); ¹³C NMR (100 MHz, CD₃OD) δ: 168.2, 152.8, 147.4, 146.1, 140.3, 139.6, 134.1, 129.1, 118.9, 118.8, 117.9, 116.5, 101.4, 95.0, 80.4, 72.9, 60.9, 58.5, 55.8, 53.4, 43.0, 25.5, 25.0; HRMS (M + H)⁺: *m/z* Calcd. for C₂₄H₂₇BrNO₁₀S, 600.0539; found 600.0511.

2.3. Predictive determination of free energy of solvation for the water-soluble noscapine analogs

Noscapinoids **1**, **2**, **4a-c**, **6a-c**, **8a-c** used in this study were solvated in cubic box of TIP3P water model and width of the box was 10 Å from the any part of the solute using the xleap module in Amber 10. All of the simulations were carried using the Amber suite of programs. The system was brought to electrostatic neutrality, if the resulting system was not already electrostatically neutral, by adding the necessary amount Na⁺ or Cl⁺ ions. The system was minimized for 1000 steps and the temperature was raised to 300 K during a 200 ps equilibration molecular dynamics simulation. An additional 5 ns of molecular dynamics simulation was carried out on each compound. Each snapshot of the 5 ns simulation trajectory was saved every 1 ps. The solvation free energies for the resulting snapshots, after stripping all of the water molecule and ions, were calculated using the MM-PBSA approach. The force field parameters for each compound were calculated as described in the *Docking and Molecular Simulation Studies* section below.

2.4. Prediction of physicochemical properties

Mavin Sketch plugin paired with JChem and ChemAxon (Budapest, Hungary) was used for the determination of the TPSA, logP, number of rotatable bonds, number of nitrogen and oxygen atoms and number of NH and OH bonds for the determination of the Lipinski's properties.

2.5. Effect of water-soluble noscapine analogs on microtubule polymerization

2.5.1. Tubulin purification

Microtubule associated proteins (MAPs) rich tubulin was purified from goat brain by two cycles of polymerization and depolymerization as described previously [15]. MAPs free tubulin was isolated by two cycles of assembly and disassembly in the presence of 1 M monosodium glutamate and 10% DMSO [15]. Protein concentration was measured by Bradford method using BSA as standard [16]. The protein was divided into aliquots and stored at –80 °C for further use.

2.5.2. Light scattering experiments

1 mg/mL of MAPs-rich tubulin in PEM buffer (25 mM Pipes, pH 6.8, 3 mM MgCl₂ and 1 mM EGTA) was incubated on ice without or with 50 μM of noscapine or its analogs for 10 min. This was followed by addition of 1 mM GTP to the reaction mixtures and the microtubule assembly was monitored at 37 °C by measuring light scattering intensity at 400 nm using a spectrofluorometer (Jasco FP-6500, Tokyo, Japan). The assembly reached a steady state within 10 min of the initiation of reaction.

Similarly, tubulin (10 μM) in 25 mM Pipes at pH 6.8 containing 3 mM MgCl₂, 1 mM EGTA and 1 M monosodium glutamate was incubated without or with different concentrations (10, 25 and 50 μM) of noscapine or its analog, **6b** on ice for 10 min and then 1 mM GTP was added to the reaction mixtures. The assembly of tubulin was monitored as described earlier.

2.5.3. GTPase activity assay

1 mg/mL of MAPs rich tubulin in PEM buffer (25 mM Pipes, pH 6.8, 5 mM MgCl₂ and 1 mM EGTA) was incubated on ice with different concentrations (0, 10, 25, 50 and 75 μM) of noscapine analog, **6b** for 10 min. The polymerization reaction was started by adding 1 mM GTP to the reaction mixtures, followed by incubation at 37 °C in the water bath. After 10 min of polymerization, the GTP hydrolysis reaction was quenched by adding 10% (v/v) of 7 M

perchloric acid to the samples. The amount of inorganic phosphate released was measured by using malachite green ammonium molybdate assay [17,18]. The same assay was performed with noscapine (0, 10, 25, 50 and 75 μM) and podophyllotoxin (0, 3, 5 and 10 μM) as controls. Similarly, 10 μM tubulin in PEM buffer (25 mM Pipes, pH 6.8, 3 mM MgCl_2 and 1 mM EGTA) was incubated on ice with 1 M monosodium glutamate and 50 μM **6b** for 10 min. The polymerization reaction was started by adding 1 mM GTP to the reaction mixture and incubating it at 37 °C in the water bath. Samples were collected at different time points (0, 2, 5, 7, 10 and 15 min) and the GTP hydrolysis was measured as described above.

2.6. Docking and molecular simulation studies

The three-dimensional crystal structure of tubulin were taken from the PDBID 1SAO [19] (3.58 Å) to apply docking and molecular dynamics simulations. The crystal structure has four chains in which chains A, B were considered and missing residues in the crystal structure were added using swiss-model webserver [20]. The initial conformations of ligand-tubulin (ligands: **1**, **2**, **6b**, **8b**, **8c**) complexes for the molecular dynamics simulations were obtained by docking ligands (**1**, **2**, **6b**, **8b**, **8c**) onto tubulin active site. The natural substrate CN2 was removed from the tubulin crystal structure and CN2 binding site was used as active site for ligands. All ligands were constructed in Gauss View 3.09 [21] and Autodock Vina [22] was used for docking calculations. Autodock ADT was used to assign Gasteiger charges to the ligands and tubulin molecules. Tubulin was rigid and ligands were flexible during docking calculations using following parameters: the grid spacing was 1.0 Å; the box size was 25 Å in each dimension, and the center of the box was chosen as the center of tubulin active site and have large enough space to sample all possible ligand conformations within the box. The maximum number of binding modes saved was set to 10. The conformation with the lowest binding energy was used and assumed to be the best binder. The lowest binding energy complex conformation was used for molecular dynamics simulations.

AMBER 10 suite of programs [23] were used to carry out the simulations in explicit TIP3P [24] water model in a periodic octahedron box, using the all-atom Cornell et al. [25] force field and the reoptimized dihedral parameters for the peptide ω -bond [26]. For ligand molecules, the partial atomic charges are derived using standard two-step RESP method from electrostatic potential calculated using Gaussian03 program [27] at HF/6-31(d, p) level of theory and generalized amber force field (gaff) parameters [28] are used. The TIP3P [24] water model was used to solvate the complexes (tubulin-ligand) in a periodic octahedron box, width of the solvent box is 10 Å away from the any part of the complex, and neutralized with Na^+ ions. Each complex was simulated for at least 30 ns, and the first 10 ns were considered for equilibration. The Newton's equation of motion was solved with an integration time step of 0.002 ps. The long-range electrostatic interaction were evaluated with the Particle Mesh Ewald method [29] and for non-bonded interactions a cutoff of 9.0 Å was used. All bonds involving hydrogen atoms were restrained using the SHAKE algorithm [30]. The simulations were carried out at a temperature of 300 K and a pressure of 1 bar. The Langevin thermostat method was used to regulate the temperature with a collision frequency of 1.0 ps^{-1} . The trajectories were saved every 500 steps (1 ps). The molecular mechanics Poisson-Boltzmann (or Generalized Born) surface area (MM-PB(GB)SA) method [31] was used to calculate the binding energy of each conformation generated during the MD simulations. The binding energies were obtained by using MM-PBSA module in AMBER 10. Generalized Born (GB) method was used to calculate the binding energy of conformations in an interval of four from each trajectory.

2.7. Cell culture and drug treatment

All culture medium was supplemented with 10% fetal bovine serum (FBS) and 1% penicillin/streptomycin. Human prostate cancer (PC-3) cells were grown in RPMI. Cervical (HeLa), pancreatic (MIA PaCa-2) and bladder (T24) were grown in DMEM.

2.7.1. In vitro cell proliferation assay

MTT assay was used to measure the percent cell proliferation of cells in vitro. 100 μL of medium containing 5×10^3 cells in density were seeded in a 96 well plates and incubated overnight. Once the cells attached, they were treated with ascending concentrations of 0, 0.01, 0.1, 1, 10, 25, 50, 100, 250 and 500 μM of noscapine analogs dissolved in PBS. Dilutions were made in media respective to the cell lines used. After 48 h incubation, the drug-containing medium was removed and fresh 90 μL of medium with 10 μL (5 mg/mL in PBS) of MTT (3-(4, 5-dimethylthiazol-2-yl)-2, 5-diphenyltetrazolium bromide) dye was added to each well followed by a 4 h incubation. The formazan product was dissolved by adding 100 μL of 100% DMSO after removing the medium from each well. The absorbance was measured at 570 nm using a Spectra Max Plus multi-well plate reader (Molecular Devices, USA).

2.7.2. Immunofluorescence confocal microscopy

PC-3 cells were grown on glass coverslips and treated with **6b**, **8b** and **8c** at 50 μM for 12 h and 24 h on coverslips. All treated cells were fixed in ice-cold (-20°C) methanol for 10 min followed by a wash with PBS. After washing, cells were blocked with 2% Bovine Serum Albumin (BSA) in PBS and incubated at 37 °C for 1 h. Fixed slides were first stained with primary α and γ tubulin from Sigma (St. Louis, MO) antibody (1:1000 dilution) and then incubated for 45 min at 37 °C. These slides were then stained with conjugated secondary antibody (1:1000 dilutions) Alexa-Fluor 488 from Life Technologies (Grand Island, NY) and Alexa-Fluor 555 from Invitrogen (Carlsbad, CA) and incubated for 45 min at 37 °C. Finally, these slides were stained with DAPI from Invitrogen (1:1000 dilution) to visualize DNA and mounted with Prolong-Gold antifade reagent. Slides were imaged using a confocal microscope.

2.8. In silico evaluation of the ADMET profile

The Absorption, Distribution, Metabolism, and Excretion (ADME) studies provide further insight into the pharmacokinetic properties of the water-soluble noscapine compounds. Furthermore, toxicity prediction including mutagenicity and carcinogenicity provides a means to estimate the toxicological potency of these analogs. Computational methods are currently used for virtual screening in lead optimization considering the enhanced accuracy of *in silico* ADMET (ADME-Tox) predictions. ADMET is used in evaluating various properties of novel leads that include solubility, blood brain barrier (BBB) penetration, cytochrome p450 (CYP) metabolism, hepatotoxicity, intestinal absorption and plasma protein binding (PPB), logP values and polar surface area (PSA). In the current study, TOPKAT[®] (Toxicity Prediction by Komputer Assisted Technology) in Accelrys Discovery Studio (version 3.5) was used to execute the ADMET prediction studies for all the analogs.

2.9. Pharmacokinetic studies

2.9.1. Sample preparation for in vivo PK studies

Required amounts of **6b**, **8b**, **8c** and noscapine were weighed and dissolved in required volume of water, vortex mixed and sonicated for 5 min. Pharmacokinetic studies were performed in male CD-1 mice following a single oral (PO) administration of **6b**,

8b, **8c** and noscapine at 50 mg/kg and intravenous (IV) dose administration at 5 mg/kg. All animals were acclimatized for 3 days before dosing in the experimental area. Mice were fasted for 3 h before dose administration and food was provided 3 h post dose. Water was provided *ad libitum* throughout the study period. Animals were marked and housed (three per cage) in polypropylene cages and maintained in controlled environmental conditions with 12 h light and dark cycles. The temperature and humidity of the room was maintained between 22 ± 3 °C and 30–70%, respectively, and approximately 10–15 fresh air change cycles per hour. A sparse sampling design was used to collect blood samples (~200 μ L) through retro-orbital plexus at 5 min, 10 min, 15 min, 30 min, 1 h, 2 h, 4 h, 6 h, 8 h, 12 h and 24 h into K_2 EDTA coated tubes. Plasma was harvested from blood by centrifugation of samples at 8000 g for 10 min. All samples were stored at -80 °C until bioanalysis.

2.9.2. Bioanalysis

All samples were processed by protein precipitation method. An aliquot (50 μ L) of plasma sample was added with 20 μ L internal standard (7-hydroxy noscapine), 180 μ L ACN, and vortex mixed for 3 min. The tubes were centrifuged at 8000 g for 10 min and an aliquot of supernatant was transferred into auto-sampler vials for analysis. The stock solutions of **6b**, **8c**, **8b**, noscapine and 7-hydroxynoscapine (internal standard) were prepared in water at 10 mg/mL. A calibration curve range of 1 ng/mL to 1 μ g/mL was employed for the quantification of analytes and internal standard concentration was 0.2 μ g/mL for each analysis. The calibration curve consisted of blank, blank with internal standard and 10 non-zero calibration standards. The calibration standards were within $\pm 15\%$ of the nominal concentration at all concentrations except lower limit of quantification, which was accepted at $\pm 20\%$ of nominal.

All samples were analyzed using liquid chromatography tandem mass spectrometric method (Agilent 6410 series). A positive ionization mode with multiple reaction monitoring (MRM, *m/z* Q1/Q3) of **6b** (*m/z* 536/220, RT 2.0 min), **8b** (*m/z* 614/300, RT 3.3 min), **8c** (*m/z* 600/300, RT 2.9 min), noscapine (*m/z* 414/220, RT 3.6 min), IS (*m/z* 220/205, RT 1.0 min) was employed. The ion spray voltage was set at 3000 V, ionization temperature set as 200 °C and drying gas flow rate was 10 L/min. Data acquisition and quantification were performed using Mass Hunter software (Agilent Technologies). Separation was achieved using HP1100 series LC (Agilent Technologies, Wilmington, DE) equipped with a photodiode array (PDA) detector, using Zorbax reversed-phase SB-C18, 2.1×50 mm, 5.0 μ m (Agilent) column. An isocratic elution method was employed to separate the water-soluble noscapine analogs using mobile phase A (80%, 0.1% formic acid in water) and mobile phase B (20%, ACN) at a flow rate of 0.25 mL/min and an injection volume of 10 μ L.

2.9.3. Pharmacokinetic analysis

Pharmacokinetic parameters were calculated from the concentration-time data using the non-compartmental analysis tool of WinNonlin[®] software (Version 5.2, Pharsight, USA). The area under the concentration time curve (AUC_{last} and AUC_{inf}) was calculated by the linear trapezoidal rule. Following oral administration, peak concentration (C_{max}) and time for the peak concentration (T_{max}) were the observed values. The clearance (CL) and volume of distribution (V_{ss}) were estimated following intravenous dose administration. The elimination rate constant value (k) was obtained by linear regression of the log-linear terminal phase of the concentration-time profile using at least three declining concentrations in terminal phase with a correlation coefficient of >0.8 . The terminal half-life value ($T_{1/2}$) was calculated using the equation $\ln 2/k$. Oral bioavailability was calculated by taking the

ratio of dose normalized AUC_{last} following oral administration to intravenous administration.

3. Results

Given the challenges posed by limited water solubility of the currently available noscapine analogs for *in vivo* efficacy experimentation and pharmacokinetic studies, the key goal of this study was to enhance the water solubility of noscapine by appropriate chemical maneuvers. To this end, we strategized to introduce charged moieties in noscapine, a highly hydrophobic molecule. We designed a total of nine novel noscapine analogs (Scheme 1) by rationally selecting two charged groups, a positively charged quaternary ammonium group, and a negatively charged sulfonate moiety for introduction on the noscapine nucleus.

3.1. Synthesis of water-soluble noscapine analogs

Our synthetic strategy first focused on the preparation of 9-aminonoscapine **3**, from the previously reported 9-bromonoscapine [12]. The conversion involved a one-pot synthesis and thus avoided the use of overly harsh and harmful reagents such as tin chloride and thiophenol, which have been used earlier for the synthesis of similar molecules. In addition, these reagents do not alter the stereogenic centers of the molecule. Bromonoscapine **2** was subjected to a copper-assisted aromatic substitution reaction with sodium azide, while using *L*-proline as the ligand to obtain the amino compound [32]. The 9-amino noscapine **3** obtained was utilized for the introduction of charged species by functionalizing the amino group as outlined in Fig. 3, to impart the highly desirable polarity and aqueous solubility to the molecule. The amino compound **3** reacted with the quaternary ammonium alkyl bromide using optimum conditions for the *N*-alkylation of aromatic amines resulting in good conversion to the desired positively charged 9-quaternary ammonium alkylamino noscapine **4a**. Correspondingly, the amino compound was also reacted with alkyl sultones, specifically 1,4-butane sultone and 1,3-propane sultone, by refluxing in *i*-propanol to introduce the negatively charged alkyl sulfonate groups on the amino functionality, to obtain the desired compounds **4b** and **4c**.

Next, we attempted functionalizing other nucleophilic positions of the molecule using the 7-dealkylated noscapine precursor, which contains a convenient hydroxyl position for the introduction of charged species for attaining improved aqueous solubility. The parent molecule was first subjected to demethylation reaction according to the method reported previously by our group to afford the 7-hydroxy noscapine. The obtained 7-hydroxy noscapine **5** reacted with the quaternary ammonium alkyl halide under phenolic alkylation conditions through the treatment of potassium carbonate at slightly elevated temperatures to yield the positively charged analog **6a** (Fig. 1). The hydroxy compound reacted with the alkyl sultones to obtain the negatively charged analogs **6b** and **6c**; however, the desired conversions were non-effective using potassium carbonate and sodium hydride was used to effect the conversion in good to excellent yields. A previous modification to the noscapine core was the addition of the 9-bromo moiety which showed improved biological efficacy; therefore, we also wanted to directly compare the results of adding water-solubilizing groups to the 9-bromonoscapine **2** core to study the ability of the charged species to impart aqueous solubility and improve the biological results. Hence we first subjected intermediate **2** to the previously employed demethylation conditions to obtain 9-bromo-7-hydroxy noscapine **7**. Compound **7** was then subjected to reaction conditions as in case of compounds **6a**, **6b** and **6c** to obtain the 9-bromo-7-O-alkylated compounds **8a**, **8b** and **8c** in excellent yields.

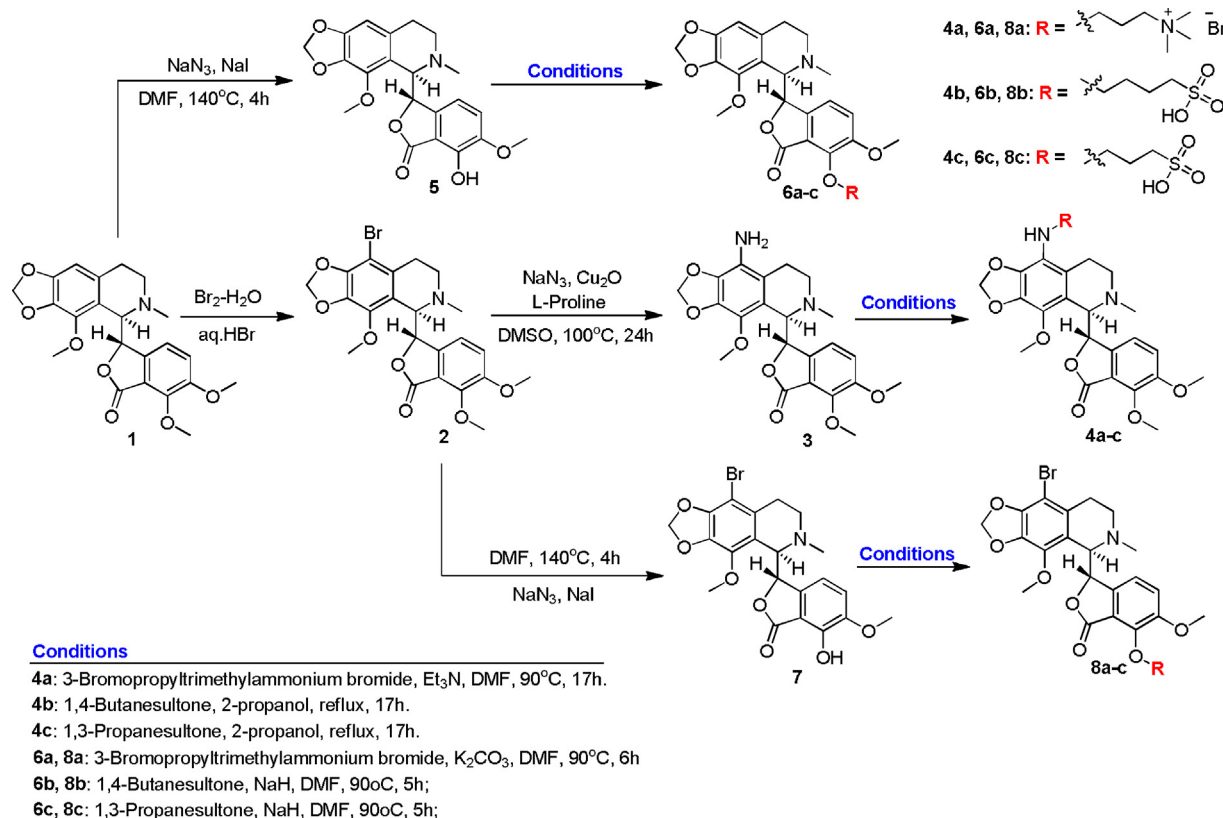


Fig. 1. Synthesis of water-soluble analogs of noscapine.

3.2. Predictive in silico studies

3.2.1. Quantitative estimation of solvation free energy

Next, we estimated solvation free energies for all nine compounds using the Poisson–Boltzmann electrostatics. Molecular dynamics simulation on each compound was performed in explicit water, and the free energy of solvation for each resulting

conformation was calculated by solving the linear Poisson–Boltzmann equation. The distribution of solvation free energies for all of the compounds is shown in Fig. 2. Noscapine (1) and bromonoscapine (2) with the most unfavorable solvation free energies were predicted to display least solubility in solution. Interestingly, our results suggested that the compounds with negatively charged alkyl-sulfonato group (4b, 4c, 6b, 6c, 8b and 8c)

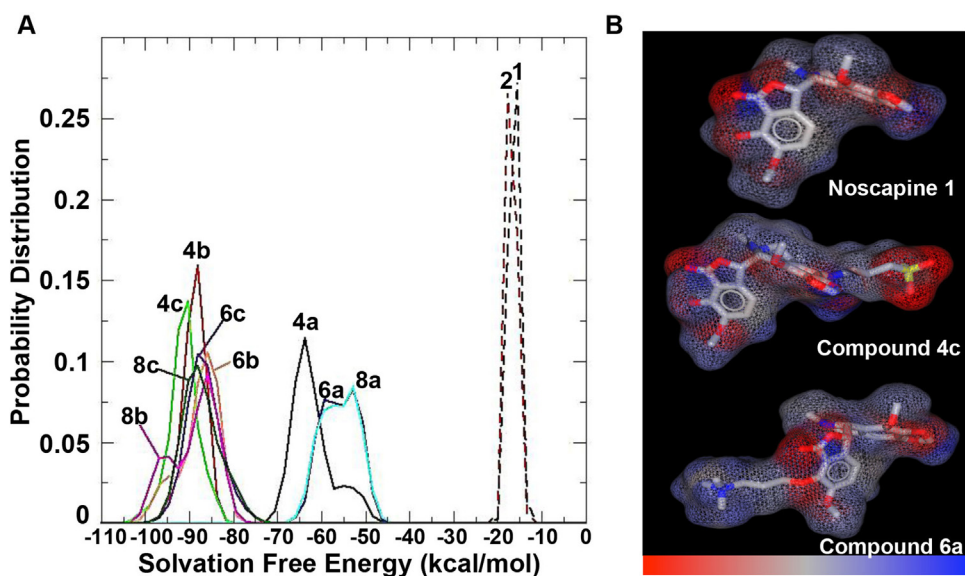


Fig. 2. (A) Diagram showing the difference in solvation free energy for the individual compounds 4a–c, 6a–c and 8a–c compared to the noscapine 1 and bromonoscapine 2 (B) Charge to hydrophobicity depictions of the compounds 1, 4c and 6a showing that the sulfonato group bearing compounds display a higher magnitude of charge compared to those that contain quaternary ammonium moiety (negative charge shown by red color in 4c versus positive charge shown by blue color in 6a, grey color signifies neutrality). (For interpretation of the references to color in this figure legend, the reader is referred to the web version of this article.)

Table 1
Physicochemical descriptors of novel noscapine analogs.

Compound	logP	TPSA	O, N atoms	Rotatable Bonds	OH, NH bonds	Mol. wt.
Noscapine	2.54	75.69	8	4	0	413.42
2	3.34	75.69	8	4	0	492.32
5	3.04	86.69	8	3	1	399.40
7	3.84	86.69	8	3	1	359.27
4a	-2.10	87.82	10	9	1	528.63
4b	-0.22	144.92	12	10	2	564.61
4c	-0.73	144.92	12	9	2	550.59
6a	-1.55	75.69	9	8	0	499.58
6b	0.04	132.89	11	9	1	535.57
6c	-0.47	132.89	11	8	1	521.54
8a	-0.74	75.69	9	8	0	578.48
8b	0.63	132.89	11	9	1	614.47
8c	0.11	132.89	11	8	1	600.44

ChemAxon (Budapest, Hungary), J Chem Plugin and Marvin were utilized to perform calculations.

were the most soluble ones. Although the amino-substituted compounds (**4a**, **6a**, and **8a**) are more soluble than **1** and **2**, they are not as soluble as the sulfonate substituted compounds. In general, all of the compounds can be classified into three clusters as shown in Fig. 2A. The distributions of solvation free energies of all the sulfonate compounds resulted in one cluster and another cluster constituted the amino compounds. Noscapine and bromonoscapine were found to be equally soluble based upon this estimation of solvation energies.

The charge-to-hydrophobicity maps (Fig. 2B) correlated strongly with the solvation free energy diagram and showed an elevated magnitude of charge density for the sulfonate modified compounds. This is clearly demonstrated by the distinctively vibrant red color compared to the faint (low charge density) blue around the quaternary ammonium group. We envision that adequate charge balancing over the entire surface offered by sulfonate group efficiently shielded the hydrophobicity (Fig. 2B). The predicted values of logP and TPSA (Table 1) strongly suggest that the charged species introduced on the noscapine moiety remarkably impacted physicochemical descriptors of the molecules. With the introduction of positively or negatively charged species, there was a huge reduction in logP and an increase in TPSA, thus indicating the basis of solubility of these compounds.

3.3. Effects of noscapine compounds on the polymerization of tubulin

We next evaluated the effect of noscapine analogs on tubulin assembly using two systems: MAPs rich tubulin and pure tubulin to establish that tubulin itself was interacting with the test agents. Among the total of nine compounds tested for their effects on tubulin polymerization, we found compounds **6b**, **8b** and **8c** to be the most effective noscapine analogs in decreasing the polymerization of MAPs-rich tubulin. The percent decrease in the MAPs-rich tubulin polymerization at 50 μ M concentrations of compounds tested was highest for **6b** ($74 \pm 13\%$) followed by **8b** ($68 \pm 18\%$) and **8c** ($61 \pm 21\%$) (Table 2). Interestingly, compound **6b** decreased the polymerization of pure tubulin as well but to a lesser extent as compared to the decrease in the MAPs-rich tubulin assembly. At 50 μ M concentration of **6b**, the decrease in light scattering of pure tubulin was only $35 \pm 7.2\%$ (Table 3). The presence of 4-oxy-butane-1-sulphonic

Table 2
Percent decrease in light scattering for noscapine analogs of MAP-tubulin.

Compound	50 μ M	Compound	50 μ M	Compound	50 μ M
1	11 ± 4	6a	19 ± 6	8a	30 ± 12
4a	29 ± 5	6b	74 ± 13	8b	68 ± 18
4b	30 ± 9	6c	32 ± 14	8c	61 ± 21
4c	27 ± 10				

acid and 4-oxy-propane-1-sulphonic acid groups on the benzofuran ring of the parent noscapine structure may be responsible for the inhibition of MAPs-rich tubulin assembly. It has been previously shown that bromonoscapine decreases the assembly of tubulin more effectively compared to parent noscapine. Thus, the presence of bromine at position 9 in **8b** and **8c** may contribute to the depolymerizing effect on MAPs-rich tubulin shown by the presence of 4-oxy-butane-1-sulphonic acid and 4-oxy-propane-1-sulphonic acid groups. This is in line when the depolymerizing effects of **6c** and **8c** are compared. Both these compounds have same structure except the presence of bromine at position 9 in **8c**, which perhaps confers an inhibitory effect on tubulin polymerization.

3.3.1. Effects of compound 6b on the GTPase activity of tubulin

Here on, we focused our biochemical assays on compound **6b** owing to its greater tubulin depolymerizing activity. We found that in the presence of different concentrations of **6b**, the GTPase activity of MAPs-rich tubulin increased significantly. The number of moles of inorganic phosphate released per mole of tubulin after 10 min of assembly increased from 62 ± 1.7 in control to 122 ± 1.4 , when MAPs rich tubulin was polymerized in presence of 75 μ M **6b** (Fig. 3A). However, when the same reaction was performed in presence of noscapine, the GTPase activity of MAPs-rich tubulin remained almost unchanged (Fig. 3A). Podophyllotoxin was included as our control and as expected, the GTPase activity of MAPs-rich tubulin decreased in the presence of different concentrations of podophyllotoxin (Fig. 3B). Intriguingly, the GTPase activity of pure tubulin did not change significantly at 50 μ M concentration of **6b**, as compared to control. After 15 min of polymerization, the number of moles of inorganic phosphate released per mole of tubulin in presence of 50 μ M concentration of **6b** was 35 ± 1 whereas it was 30 ± 1.5 in case of control (Fig. 3 C).

3.4. In silico docking and molecular simulation studies

We next decided to perform molecular simulations and *in silico* docking studies to gain insights into how the three compounds (**6b**, **8b** and **8c**) as well as our two well-researched molecules used as

Table 3
Percent decrease in light scattering of pure tubulin.

Compound ID	Concentration (μ M)	% Decrease in light scattering
1	10	5 ± 1.5
1	25	9 ± 2.6
1	50	13 ± 2.9
6b	10	14 ± 6
6b	25	25 ± 7.6
6b	50	35 ± 7.2

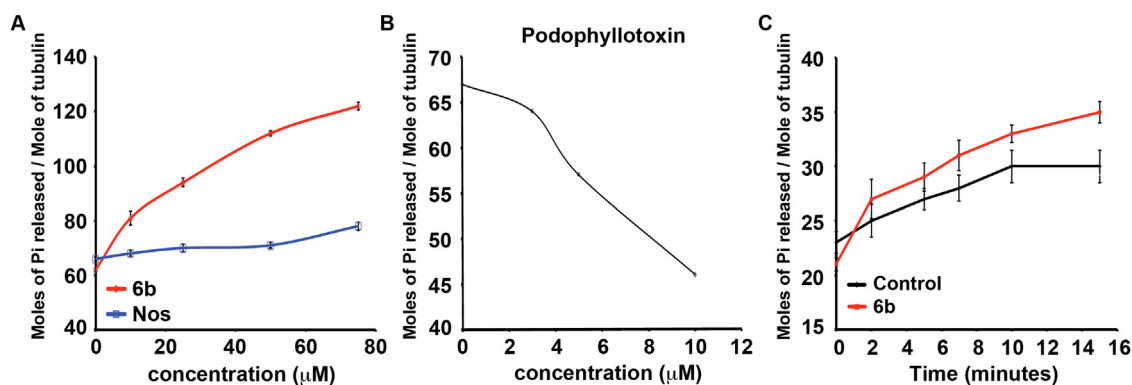


Fig. 3. Effect of **6b** on the GTPase activity of MAPs rich and pure tubulin. (A) Change in the GTPase activity of MAPs rich tubulin in presence of different concentrations of **6b** (red) and noscapine (blue). The data is average of three sets of experiments. (B) Decrease in the GTPase activity of MAPs rich tubulin in presence of different concentrations of podophyllotoxin. (C) GTPase activity of pure tubulin in absence (black) or presence of 50 µM **6b** (red). The data is an average of three sets of experiments. (For interpretation of the references to color in this figure legend, the reader is referred to the web version of this article.)

study standards—namely noscapine and bromonoscapine, docked into the active site independently at the interface of the alpha and beta domains of the tubulin dimer. The binding orientations were held similar for all of the ligand-tubulin complexes. The docking results suggest that noscapine structure can be divided into two distinct halves (a) the tetrahydroisoquinoline moiety which can insert deep and interact closely with the tubulin dimer, whereas (b) dimethoxyisobenzofuranone group gets closer to GTP in ligand-tubulin docked complex. (Fig. 4A, B, C, D, E). These initial docked complexes were used as the starting conformation for

further studies using molecular dynamics simulations and free energy calculations. Each complex was simulated for at least 30 ns in explicit water. The free energy of binding the ligand into the active site was calculated for each resulting snapshot from the molecular dynamics simulations. Distributions of the binding free energies for all of the five compounds are shown in Fig. 4F. Our *in silico* modeling results suggested that compound **8b** has the strongest affinity for the tubulin dimer. In general, the bromo-substituted compounds adopted a similar binding configuration in the active site, which is different from the un-substituted

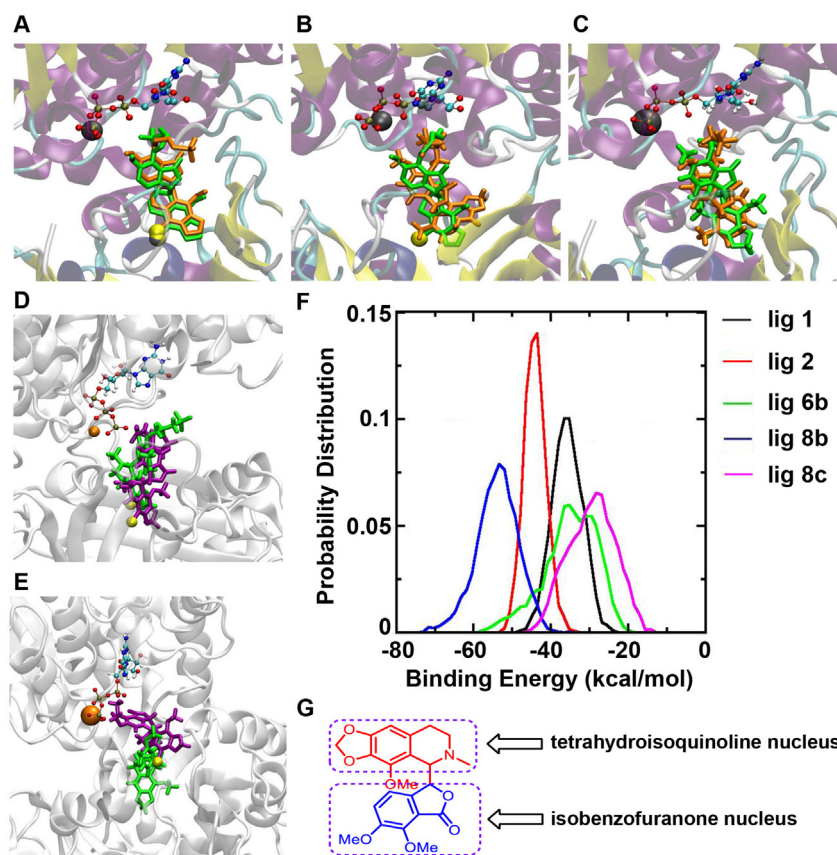


Fig. 4. Docked conformations of ligands in tubulin active site (A) **1** (green) & **6b** (orange); (B) **6b** (orange) & **8b** (green); (C) **8b** (green) & **8c** (orange). Conformations obtained after 30 ns simulation of ligand-tubulin complex; (D) **8b** (purple) & **8c** (green); (E) **1** (green) and **2** (purple) GTP was shown in ball and stick model, Mg²⁺ ion VDW model in orange color, Br-atom in yellow color in VDW model. (F) Binding energy (kcal/mol) of ligands **1**, **2**, **6b**, **8b**, and **8c**. (G) Molecular structure of noscapine highlighting the tetrahydroisoquinoline and the dimethoxyisobenzofuranone moiety. (For interpretation of the references to color in this figure legend, the reader is referred to the web version of this article.)

compounds. Interestingly, the compound with the longer side chain (**8b**) docked better in the active site as it plausibly allowed the sulfate group to move away from the phosphate group of GTP compared to the compound with a shorter side chain (**8c**). These data suggest that the bromo-substituted compound with a longer side chain (4-carbon) is showed optimal binding characteristics.

For the different drug-tubulin complexes, we also calculated the distance between the center of mass between the two domains (alpha and beta subunits) and the angle defined by the two domains during the molecular dynamics simulations. All of the complexes showed similar domain-domain distances, with a slightly longer distance exhibited by compound **8c** towards the end of the simulations. Similarly, all of the complexes exhibited similar domain-domain angle, with slightly larger angle for compounds **6b** and **8c**. Our results suggested that the steric hindrance imposed by **8c** pushes the two domains apart. Therefore, even though, compound **8c** is shown to bind with weaker affinity, it might still be able to effectively destabilize the interactions between the two domains (alpha and beta subunits of tubulin dimer) (data not shown).

3.5. In vitro efficacy of water-soluble noscapine analogs

3.5.1. Water-soluble noscapine analogs inhibit proliferation of cancer cells more potently than noscapine and bromonoscapine

The newly synthesized water-soluble noscapine analogs were evaluated for their antiproliferative activity in PC-3, a human prostate cancer cell line using the MTT assay. Essentially, the idea was to compare the differential effect of (a) propyl trimethylammonium group, (b) butyl sulfonato and (c) propyl sulfonato water-soluble side chains of these water-soluble noscapine analogs on the antiproliferative activity compared to noscapine and bromonoscapine. The three final classes are derived from their original noscapine backbone and include 9-aminonoscapine derivatives **4a–c**, 9-hydroxynoscapine analogs **6a–c**, and 9-bromonoscapine based compounds **8a–c**. For comparison, noscapine and bromonoscapine standards were prepared similarly in water and filtered for use subsequent to sonication.

Fig. 5 shows line-plots of percent cell survival versus gradient concentrations of the nine water-soluble noscapine analogs along with the two standards to yield IC_{50} values of each analog in PC-3

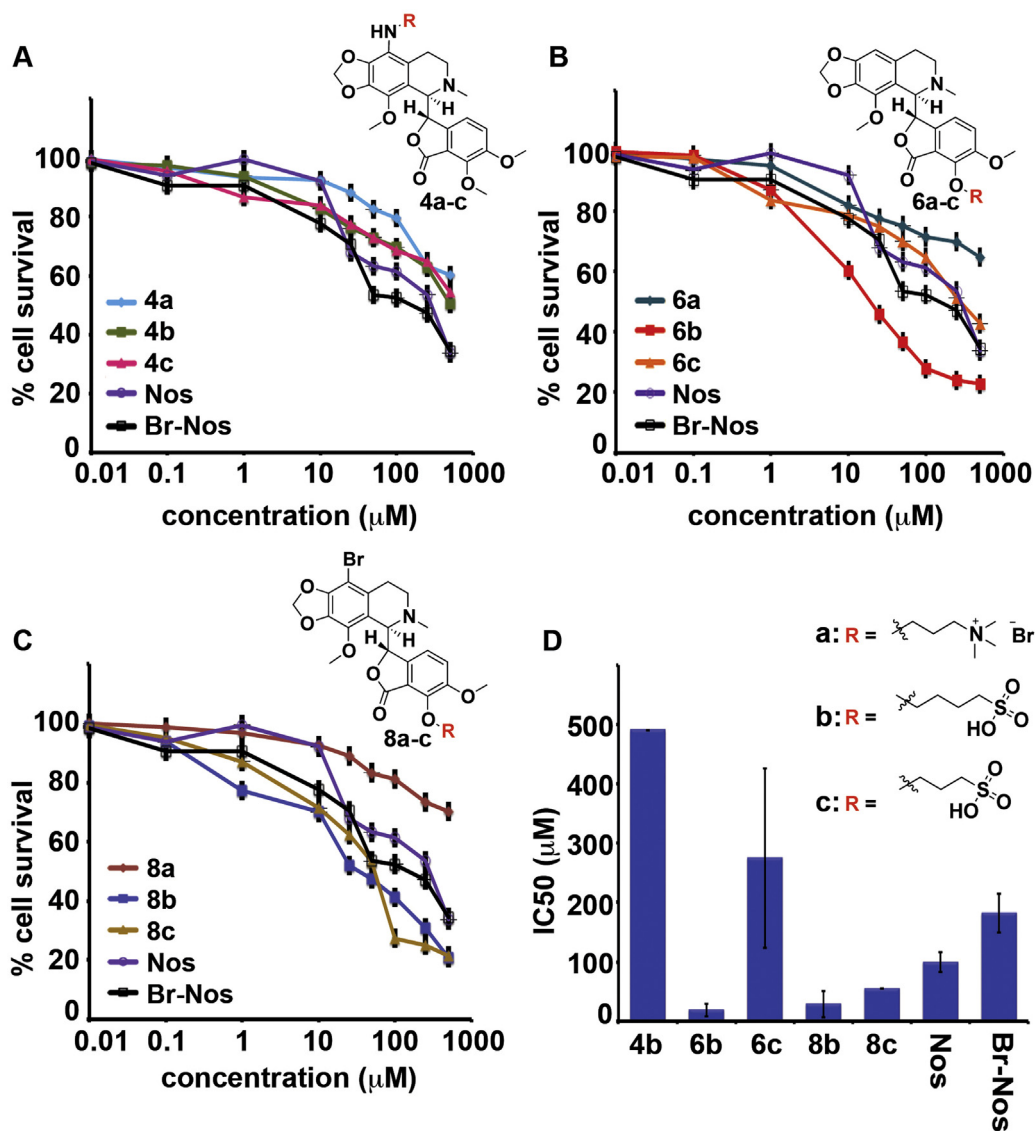


Fig. 5. PC-3 cells were treated for 48 h with increasing concentration of noscapine and its nine water-soluble analogs to measure the percentage cell proliferation using MTT assay. (A) Line graph represents percent cell survival upon treatment with noscapine analogs **6a–c**. (B) Upon treatment with noscapine analogs **4a–c**. (C) Upon treatment with noscapine analogs **8a–c**. (D) Bar-graph represents the IC_{50} (µM) values of all the noscapine analogs. The IC_{50} value of **4a**, **4c**, **6a** and **8a** were not determined.

Table 4
Comparison of IC₅₀ (μM) values of water-soluble noscapine analogs in PC-3 cells.

Analog	4a	4b	4c	6a	6b	6c	8a	8b	8c	Nos	Br-Nos
IC ₅₀ (μM)	ND	490	ND	ND	19	275	ND	29	55	100	182

ND: not determined.

cells. Analogs of amino substituted compounds **4a–c** (Fig. 5A, Table 4) showed least activity, with **4a** and **4c** displaying high IC₅₀ values after 48 h of treatment; similarly, analog **4b** showed an IC₅₀ value of 490 μM which was much higher than that of noscapine suggesting that the intended modification at this particular position is detrimental to the efficacy of the parent compound. Among the second subclass of analogs with alkylated hydroxyl group obtained from the cleaved methyl ester, **6b** displayed highest antiproliferative activity with an IC₅₀ of 19 μM (Fig. 5B, Table 4). The brominated analogs **8b** and **8c** (Fig. 5C, Table 4) displayed an IC₅₀ value of 29 and 55 μM, respectively. Analogs with the quaternary ammonium substituent imparted negligible effects on the proliferation of cancer cells. The IC₅₀ value (drug concentration at which 50% inhibition of cell proliferation occurs) of these synthesized compounds are presented in Fig. 5D, and Table 4.

Having screened all the nine water-soluble noscapine analogs in PC-3 cells, we narrowed down to evaluate the inhibition of cellular

proliferation for the most active analogs **6b**, **8b** and **8c** in other representative cancer cell lines of varying tissue origin (Fig. 6, Table 5). For this experiment, we included HeLa (cervical), MIA-PaCa-2 (pancreatic) and T24 (bladder) cancer cells (Fig. 6A, B, C, Table 5). Our data suggest that T24 bladder cancer cells were most sensitive to these three analogs and exhibited IC₅₀ values of 3.3, 32, 4 μM for **6b**, **8b**, **8c**, respectively (Fig. 6C, Table 5). Interestingly, HeLa cells (Fig. 6A, Table 5) were least responsive to these analogs with IC₅₀ values of 66, 53 and 53 μM with **6b**, **8b**, **8c**, respectively. Noscapine and 9-bromonoscapine resulted in poor activity in all three cell lines compared to **6b**, **8b** and **8c**.

3.5.2. Water-soluble noscapine analogs impede the cell cycle by inducing mitotic arrest with aberrant figures

We next examined the effects of these most-active water-soluble noscapine analogs (**6b**, **8b** and **8c**) on the cell cycle by employing immunofluorescence confocal microscopy. PC-3 cells

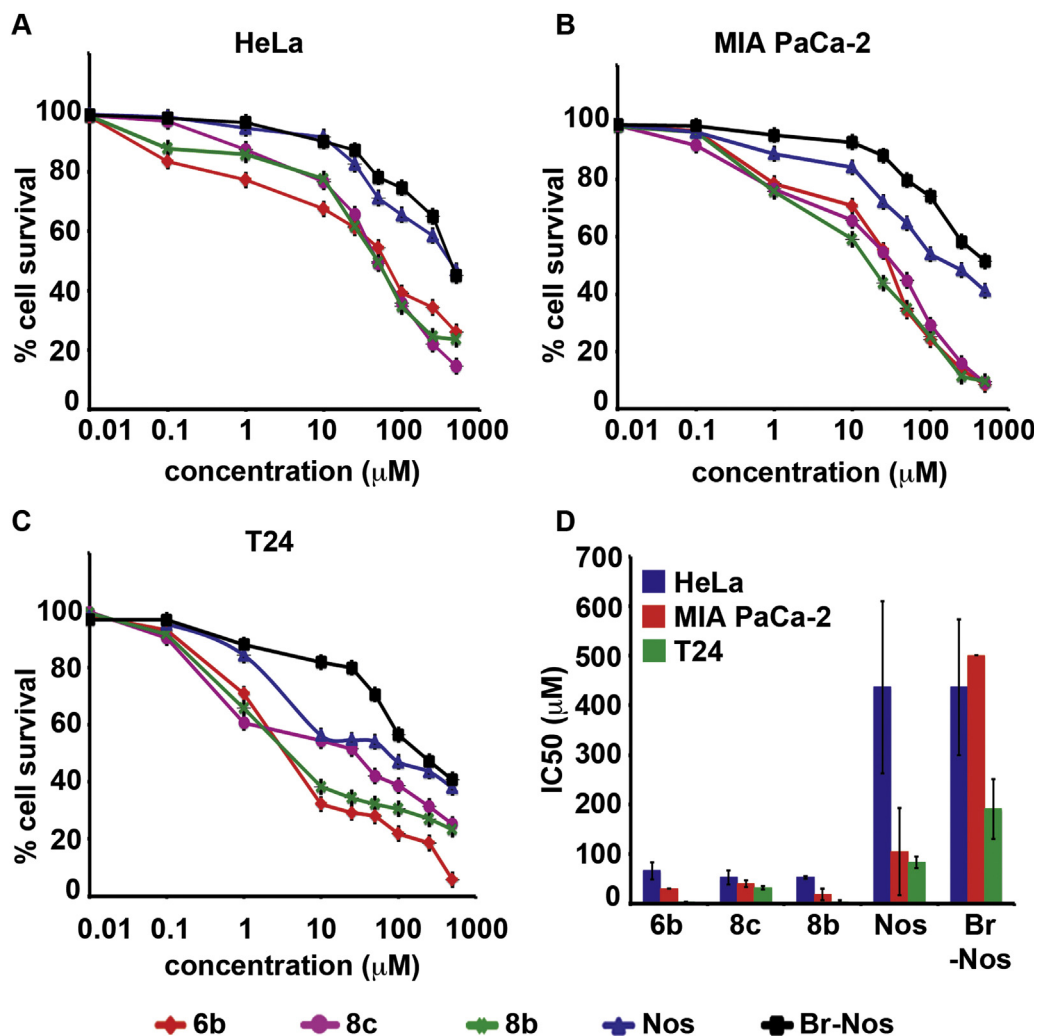


Fig. 6. Various cancer cell lines were treated with noscapine (Nos) and its most active water-soluble analogs namely **6b**, **8b** and **8c** for 48 h to measure percentage cell proliferation using MTT assay. (A) Line graph represents the percent cell survival of treated HeLa cells. (B) Represents percent cell survival of treated MIA PaCa-2 cells. (C) Represents the percent cell survival of treated T24 cells. (D) Bar-graph represents the IC₅₀ (μM) of **6b**, **8b**, **8c**, noscapine (Nos) and 9-bromonoscapine (Br-Nos) in HeLa (blue), MIA PaCa-2 (red) and T24 (green). (For interpretation of the references to color in this figure legend, the reader is referred to the web version of this article.)

Table 5Comparison of IC₅₀ (μM) values in various cell lines.

Analog	IC ₅₀ (μM)		
	HeLa	MIA Paca-2	T24
6b	66	30	3.3
8b	53	40	32
8c	53	18	4
Nos	436	105	83
Br-Nos	436	ND	191

treated with **6b**, **8b** and **8c** at 25 μM were stained for DNA (blue), microtubules (red) and centrosomes (green) (Fig. 7). As expected, control untreated cells showed bipolar mitotic cells. However, water-soluble noscapine analogs induced centrosome amplification and spindle multipolarity, which is in agreement with the centrosome declustering activity of 9-bromonoscapine.

3.6. Water-soluble noscapine analogs are non-toxic

The water-soluble noscapine analogs were then subjected to ADMET prediction using TOPKAT and the information thus obtained concludes that all the analogs have good ADMET properties and can be considered for further evaluation. These compounds are predicted to be devoid of any mutagenic or carcinogenic properties, as all of them show negligible discriminant score (Table 6). The predicted solubility of these compounds lies in level 2 and 3, indicating that these compounds have good solubility. As the predicted values of brain-blood ratio lie within level 3 or 4, it can also be concluded that all the synthesized compounds have low brain permeation (brain-blood ratio 0.3:1) (Table 6).

Table 6 The ADMET parameters for 4(a–c), 6(a–c), 8(a–c) were calculated using TOPKAT[®] (Toxicity Prediction by Komputer Assisted Technology) in Accelrys Discovery Studio (Version 3.5). All properties and OPS (Optimum Prediction Space method) components are within expected ranges for mutagenicity (Ames PROB), and ADMET Extensible models of CYP2D6, HEPATOX, and PPB. The intestinal absorption is predicted as good to moderate for these compounds. The prediction for CYP2D6 is rated as “false” indicating that these compounds doesn't inhibit CYP2D6 and HEPATOTOX parameters were negative (Table 6) suggesting that these analogs do not exhibit hepatotoxicity, thus making them potential leads for further research.

3.7. Water-soluble noscapine analogs have improved bioavailability than noscapine

Following the administration of identical concentrations of the three active analogs, we found remarkable differences in their PK

Table 6

ADMET values of Water-Soluble Noscapine Analogs.

ADMET parameters	4a	4b	4c	6a	6b	6c	8a	8b	8c
PSA 2D	87.04	142.46	142.46	74.23	129.65	129.65	74.23	129.65	129.65
AlogP98	1.67	2.87	2.29	1.86	3.06	2.48	2.61	3.81	3.23
Solubility Level	3.00	2.00	2.00	3.00	2.00	2.00	2.00	2.00	2.00
BBB Level	3.00	4.00	4.00	3.00	4.00	4.00	3.00	4.00	4.00
Absorption Level	0.00	2.00	2.00	0.00	1.00	1.00	0.00	2.00	1.00
Ames PROB	0.05	0.14	0.12	0.03	0.07	0.10	0.02	0.05	0.08
ADMET EXT CYP2D6	-1.32	-5.27	-6.15	-3.42	-7.56	-7.63	-1.56	-6.08	-5.70
ADMET EXT HEPATOTOX	-1.43	-2.62	-2.05	-2.44	-3.32	-2.27	-2.14	-3.11	-2.51
ADMET EXT PPB	-10.31	-1.56	-1.85	-12.07	-2.83	-2.68	-10.15	-1.17	-0.83

PSA 2D, polar surface area; AlogP98, hydrophobicity parameter; Solubility level, predicts aqueous solubility level; BBB level, predicts blood brain barrier penetration; Absorption level, predicts the human intestinal absorption; Ames PROB, predicts probability of mutagenicity; CYP2D6, predicts the inhibition or non-inhibition of CYP450 2D6 enzyme; HEPATOTOX, predicts hepatotoxicity or non-hepatotoxicity; PPB, plasma protein binding.

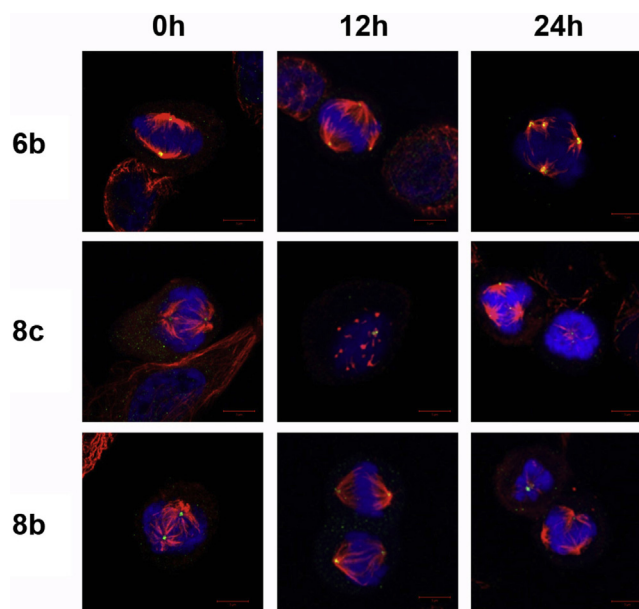


Fig. 7. **6b**, **8b** and **8c** cause spindle abnormalities the cells arrested by these analogs are showing bipolar spindles. Immunofluorescence confocal images of PC-3 cells after treatment with **6b**, **8c** and **8b** at 12 h and 24 h in comparison to control. DNA was stained using DAPI (blue), microtubule was stained using alpha-tubulin (red) and centrosomes are stained using gamma-tubulin (green). (For interpretation of the references to color in this figure legend, the reader is referred to the web version of this article.)

profiles as compared to the parent, noscapine. We evaluated the levels of **6b**, **8b**, **8c** and noscapine in the plasma following oral administration (50 mg/kg) in CD-1 mice (three mice per group). All the plasma samples were then evaluated for the presence of **6b**, **8b**, **8c** and noscapine (Fig. 8) followed by their quantitation using LC/MS/MS. To assess the bioavailability of these components, **6b**, **8b**, **8c** and noscapine were dosed individually at an intravenous dose of 5 mg/kg (Fig. 8).

The pharmacokinetic parameters were calculated using non-compartmental analysis tool of validated WinNonlin software (version 5.2). The bioavailability of **6b** is more compared to noscapine at same concentration. The C_{max} values of **6b**, **8b**, **8c** and noscapine in blood plasma samples obtained following their oral administration were compared using independent sample *t*-test. The pharmacokinetic parameters of these compounds following intravenous and oral administration were calculated (Table 7A and B). Following intravenous administration, clearance of all compounds was more than normal liver blood flow of 90 mL/min/kg). The volume of distribution of all compounds was 8–34 fold higher than normal body water of 0.7 L/kg. All compounds were rapidly

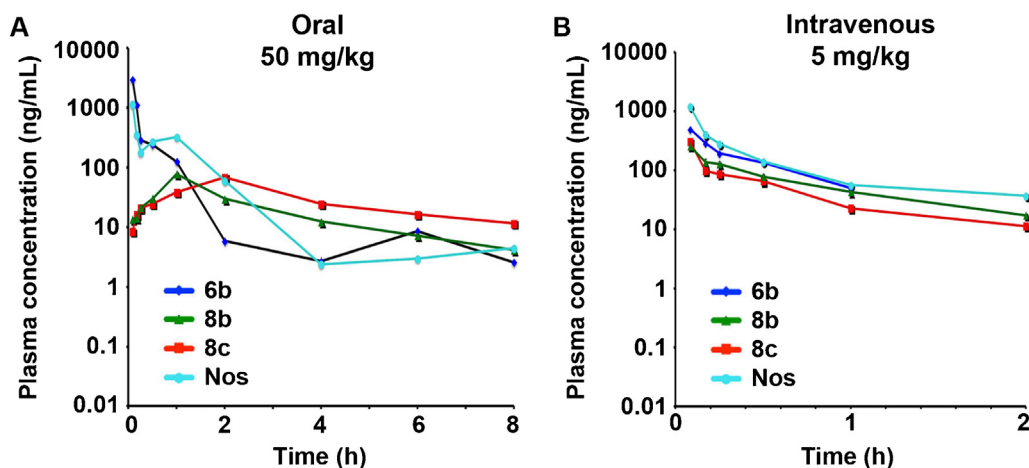


Fig. 8. Plasma concentration-time profiles of water-soluble noscapine analogs and noscapine (Nos) following their (A) oral (50 mg/kg) and (B) intravenous (5 mg/kg) administration. Error bars refer to \pm SD.

cleared with an half-life of less than 1 h. Upon oral feeding, **6b** achieved the highest C_{max} (2966.79 ± 60.06 ng/mL) compared to noscapine (1156.04 ± 18.93 ng/mL) and other analogs showed lower exposure. Interestingly, though the exposure (AUC_{last}) of **6b** was three times that of **8c** when fed orally, the bioavailability of **8c** was almost equal to that of **6b** (Table 7B). No statistical analysis was performed on AUC_{last} as it was a sparse sampling design with composite profile. Furthermore, the bioavailability of **6b** and **8c** were calculated to be higher than noscapine by 2.1 and 1.7 fold respectively (Table 7B).

4. Discussion

Noscapine and its semi-synthetic analogs are being intensely researched worldwide for their ‘kinder and gentler’ anticancer action. However, their limited water solubility impedes extensive evaluation of *in vivo* efficacy. This spurred a new line of inquiry through the utilization of cycloencapsulation methods (using beta-cyclodextrin) as well as nanodelivery approaches (using polyethylene glycol-conjugated nanoparticles). Although these modalities indicated promise, a fine-tuned control of several confounding variables and conditions confers complexity and reduces their translational impact in the clinic. We thus pondered if we could rationally strategize to introduce some charged moieties that confer water solubility on the basic noscapine backbone. Through various synthetic manipulations of the noscapine core at two distinct positions, we have been successful in synthesizing water-soluble noscapines, which conformed to the *in silico* predictions for solvation energy and physicochemical properties.

Our data underscores that the new generation water-soluble noscapine analogs demonstrated better antiproliferative activity in several human cancer cell lines compared to the previously known noscapine analogs [12–14,33]. Noscapine is a unique tubulin binding agent in that it alters microtubule dynamics without affecting the total polymer mass of tubulin, thus conforming to its microtubule-modulating characteristics [33]. In the present study, we elucidate that all novel water-soluble noscapinoids decrease the polymerization of MAPs-rich tubulin significantly as compared to noscapine and bromonoscapine. Compound **6b** was found to be the most potent inhibitor of polymerization of MAPs-rich tubulin. However, this compound did not inhibit the polymerization of pure tubulin to the same extent. Nonetheless, **6b** showed greater inhibitory effect on tubulin polymerization compared to noscapine. In addition, **6b** increased the GTPase activity of MAPs-rich tubulin considerably, whereas it negligibly affected the GTPase activity of pure tubulin.

Given that **6b** impacted the polymerization and GTPase activity of MAPs rich tubulin and pure tubulin differently, it might be possible that this compound interferes with the interaction of MAPs to the microtubule, thus destabilizing microtubules indirectly. Further investigations will be required to test this possibility. Compound **6b**-stimulated GTPase activity of tubulin may perhaps be due to the tubulin-**6b** complex, suggesting that **6b** inhibits tubulin assembly by binding to a tubulin-tubulin interaction site required for the polymerization dependent-GTPase activity. We may also propose that **6b** induces a conformational change that leads to polymerization independent GTPase activity.

Table 7

A. Pharmacokinetic parameters of water-soluble noscapine analogs following intravenous administration in CD-1 mice (dose 5 mg/kg).

Analyte	C_0 (ng/mL)	AUC_{last} (ng ² h/mL)	CL (mL/Min/kg)	V_{SS} (L/kg)	Half-life (h)
6b	502.09	197.93	369	9.53	0.63
8b	259.39	145.41	512	23.81	0.38
8c	307.09	133.46	584	18.36	0.70
Nos	1211.76	478.67	174	4.55	0.39

B. Pharmacokinetic parameters of water-soluble noscapine analogs following oral gavage administration in CD-1 mice (dose 50 mg/kg)

Analyte	T_{max} (h)	C_{max} (ng/mL)	AUC_{last} (ng ² h/mL)	Bioavailability F	Fold increase in F compared to Nos
6b	0.08	2970 ± 60	611	27	2.1
8b	0.08	14 ± 7	164	11	0.9
8c	0.08	8.5 ± 0.2	240	21	1.7
Nos	0.08	1156 ± 19	603	13	–

C_0 , back extrapolated concentration; AUC_{last} , area under the curve, CL, clearance, V_{SS} : volume of distribution at steady state; Nos, noscapine.

T_{max} , time to reach peak plasma concentration; C_{max} , peak plasma concentration, AUC_{last} , area under the curve, F, Bioavailability-calculated using dose normalized AUC_{last} , Nos, noscapine.

We further demonstrated that **6b**, **8b** and **8c** induced a multipolar phenotype in human prostate cancer PC-3 cells at concentrations much lower than noscapiene. This is consonant with the centrosome declustering activity of halogenated noscapienes that perhaps explains their ability to induce mitotic catastrophe. Furthermore, these water-soluble noscapiene analogs were predicted to have no toxicity with low brain permeation, followed by good intestinal absorption. Also, pharmacokinetic evaluation revealed that these compounds showed at least 1–2 fold improved bioavailability compared to noscapiene. Further investigation comparing their *in vivo* tumor growth inhibiting efficacy is currently underway in our laboratory. Considering the challenges of poor solubility resulting in poor absorption, which may also lower the efficacy, the enhanced bioavailability of **6b**, **8b** and **8c** could be attributed to their improved solubility and thus could even lead to better anticancer efficacy compared to noscapiene.

In conclusion, we have presented detailed synthesis and evaluation of next generation water-soluble analogs **6b**, **8b** and **8c** which are more potent than noscapiene in inhibiting proliferation of prostate, pancreatic breast and cervical cancer cells *in vitro* and even enhanced bioavailability *in vivo* with no toxicity. Given the attractive attributes of noscapiene that led to its rapid development and clinical trials, these water-soluble noscapienes generate a novel direction to merit extensive preclinical research.

Acknowledgments

Synthetic work was supported by the Georgia Research Alliance grant to MH. EAO was supported through the Center for Diagnostics and Therapeutics (CDT). The biological work was supported by grants to RA from the National Cancer Institute at the National Institutes of Health and DAE-SRC fellowship, Government of India to DP.

References

- [1] Dumontet C, Jordan MA. Microtubule-binding agents: a dynamic field of cancer therapeutics. *Nat Rev Drug Discov*. 2010;9:790–803.
- [2] Perez EA. Microtubule inhibitors: differentiating tubulin-inhibiting agents based on mechanisms of action, clinical activity, and resistance. *Mol Cancer Ther* 2009;8:2086–95.
- [3] Stanton RA, Gernert KM, Nettles JH, Aneja R. Drugs that target dynamic microtubules: a new molecular perspective. *Med Res Rev* 2011;31:443–81.
- [4] Morris PG, Fornier MN. Microtubule active agents: beyond the taxane frontier. *Clin Cancer Res* 2008;14:7167–72.
- [5] Checchi PM, Nettles JH, Zhou J, Snyder JP, Joshi HC. Microtubule-interacting drugs for cancer treatment. *Trends Pharmacol Sci* 2003;24:361–5.
- [6] New microtubule-inhibiting anticancer agents. *Expert Opin Investig Drugs* 2010;19:329–43.
- [7] Ke Y, Ye K, Grossniklaus HE, Archer DR, Joshi HC, Kapp JA. Noscapiene inhibits tumor growth with little toxicity to normal tissues or inhibition of immune responses. *Cancer Immunol Immunother* 2000;49:217–25.
- [8] Ye K, Ke Y, Keshava N, Shanks J, Kapp JA, Tekmal RR, et al. Opium alkaloid noscapiene is an antitumor agent that arrests metaphase and induces apoptosis in dividing cells. *Proc Natl Acad Sci* 1998;95:1601–6.
- [9] Aneja R, Dhiman N, Idnani J, Awasthi A, Arora S, Chandra R, et al. Preclinical pharmacokinetics and bioavailability of noscapiene, a tubulin-binding anticancer agent. *Cancer Chemother Pharmacol* 2007;60:831–9.
- [10] Aneja R, Vangapandu SN, Lopus M, Visweswarappa VG, Dhiman N, Verma A, et al. Synthesis of microtubule-interfering halogenated noscapiene analogs that perturb mitosis in cancer cells followed by cell death. *Biochem Pharmacol* 2006;72:415–26.
- [11] Anderson JT, Ting AE, Boozer S, Brunden KR, Crumrine C, Danzig J, et al. Identification of novel and improved antimitotic agents derived from noscapiene. *J Med Chem* 2005;48:7096–8.
- [12] Zhou J, Gupta K, Aggarwal S, Aneja R, Chandra R, Panda D, et al. Brominated derivatives of noscapiene are potent microtubule-interfering agents that perturb mitosis and inhibit cell proliferation. *Mol Pharmacol* 2003;63:799–807.
- [13] Aneja R, Vangapandu SN, Lopus M, Chandra R, Panda D, Joshi HC. Development of a novel nitro-derivative of noscapiene for the potential treatment of drug-resistant ovarian cancer and T-cell lymphoma. *Mol Pharmacol* 2006;69:1801–9.
- [14] Mishra RC, Karna P, Gundala SR, Pannu V, Stanton RA, Gupta KK, et al. Second generation benzofuranone ring substituted noscapiene analogs: synthesis and biological evaluation. *Biochem Pharmacol* 2011;82:110–21.
- [15] Panda D, Rathinasamy K, Santra MK, Wilson L. Kinetic suppression of microtubule dynamic instability by griseofulvin: implications for its possible use in the treatment of cancer. *Proc Natl Acad Sci U S A* 2005;102:9878–83.
- [16] Bradford MM. A rapid and sensitive method for the quantitation of microgram quantities of protein utilizing the principle of protein-dye binding. *Anal Biochem* 1976;1976.
- [17] Geladopoulos TP, Sotiroidis TG, Evangelopoulos AE. A malachite green colorimetric assay for protein phosphatase activity. *Anal Biochem* 1991;192:112–6.
- [18] Rai A, Suroliya A, Panda D. An antitubulin agent BCFMT inhibits proliferation of cancer cells and induces cell death by inhibiting microtubule dynamics. *PLoS One* 2012;7:e44311.
- [19] Ravelli RB, Gigant B, Curmi PA, Jourdain I, Lachkar S, Sobel A, et al. Insight into tubulin regulation from a complex with colchicine and a stathmin-like domain. *Nature* 2004;428:198–202.
- [20] Arnold K, Bordoli L, Kopp J, Schwede T. The SWISS-MODEL workspace: a web-based environment for protein structure homology modelling. *Bioinformatics* 2006;22:195–201.
- [21] Dennington II R, Keith T, Millam J. Gaussview, Version 309, Semichem, Inc, Shawnee Mission, KS; 2003.
- [22] Trott O, Olson AJ. AutoDock Vina improving the speed and accuracy of docking with a new scoring function, efficient optimization, and multithreading. *J Comput Chem* 2010;30:455–61.
- [23] Case DA, Darden TA, Cheatham I TE, Simmerling CL, Wang J, Duke RE, et al. AMBER 10. San Francisco: University of California; 2008.
- [24] Jorgensen WL, Chandrasekhar J, Madura JD, Impey RW, Klein ML. Comparison of simple potential functions for simulating liquid water. *J Chem Phys* 1983;79:926–35.
- [25] Cornell WD, Cieplak P, Christopher IB, Gould IR, Merz JKM, Ferguson DM, et al. A second generation force field for the simulation of proteins, nucleic acids, and organic molecules. *J Am Chem Soc* 1995;117:5179–97.
- [26] Urmi D, Hamelberg D. Reoptimization of the AMBER force field parameters for peptide bond (omega) torsions using accelerated molecular dynamics. *J Phys Chem B* 2009;113:16590–95.
- [27] Frisch MJ, Trucks GW, Schlegel HB, Scuseria GE, Robb MA, Cheeseman JR, et al. Gaussian 03. Wallingford, CT: Gaussian, Inc.; 2004.
- [28] Wang J, Wolf RM, Caldwell JW, Kollman PA, Case DA. *J Comput Chem* 2004;25:1157–74.
- [29] Darden T, York D, Pedersen L. Particle mesh Ewald: an Nlog(N) method for Ewald sums in large systems. *J Chem Phys* 1993;98:10089–92.
- [30] Ryckaert JP, Ciccotti G, Berendsen HJC. Numerical integration of the Cartesian equations of motion of a system with constraints: molecular dynamics of n-alkanes. *J Comput Phys* 1977;23:327–41.
- [31] Kollman PA, Massova I, Reyes C, Kuhn B, Huo S, Chong L, et al. Calculating structures and free energies of complex molecules: combining molecular mechanics and continuum models. *Acc Chem Res* 2000;33:889–97.
- [32] Markiewicz JT, Wiest O, Helquist P. Synthesis of primary aryl amines through a copper-assisted aromatic substitution reaction with sodium azide. *J Organ Chem* 2010;75:4887–90.
- [33] Landen JW, Lang R, McMahon SJ, Rusan NM, Yvon A-M, Adams AW, et al. Noscapiene alters microtubule dynamics in living cells and inhibits the progression of melanoma. *Cancer Res* 2002;62:4109–14.